Astron. Astrophys. 359, 514–522 (2000)

ASTRONOMY AND ASTROPHYSICS

# High-energy $\gamma$-ray emission from gamma-ray bursts

**F. De Paolis, G. Ingrosso, and D. Orlando**

Dipartimento di Fisica, Università di Lecce, and INFN, Sezione di Lecce, Via Arnesano, CP 193, 73100 Lecce, Italy

Received 17 April 2000 / Accepted 16 May 2000

**Abstract.** GRBs are nowadays a rather well understood phenomenon in the soft (KeV-MeV) $\gamma$-ray energy band, while only a few GRBs have been observed at high photon energies ($E_\gamma \gtrsim 1$ GeV). It is also widely recognized that GRBs accelerate protons to relativistic energies and that dense media are often present nearby the sources. Within this framework and by further adopting Totani's suggestion that GRB events release an amount of energy $\sim 10^{54}\Delta\Omega$ erg, we compute in detail the high-energy $\gamma$-ray flux from the decay of neutral pions produced through the interaction of accelerate protons with nucleons in the surrounding medium. We also take into account the local and intergalactic $\gamma$-ray absorption. The presence of magnetic fields around the GRB sources causes the deflection of the accelerated protons and so a temporal spread of the produced high-energy $\gamma$-rays with respect to the signal in the soft $\gamma$-ray band. Moreover, we analyze the possibility to detect the $\gamma$-ray signal in the GeV-TeV energy range by the ARGO detector under construction in Tibet.

**Key words:** gamma rays: bursts – gamma rays: theory

## 1. Introduction

Gamma-ray bursts (GRBs) have intrigued observers and confounded theorists ever since their discovery over thirty years ago. Up to now, the most meaningful contribution to the comprehension of the GRB physics has been obtained through the observations by BATSE and EGRET instruments on board of the CGRO satellite. Since 1991, BATSE detects about one GRB per day in the 50–300 keV energy band (hereafter indicated as soft $\gamma$-ray regime), with fluences between $\sim 10^{-7} - 10^{-5}$ erg cm$^{-2}$ and durations ranging from $\simeq 10$ ms to $\simeq 10^3$ s (Paciesas et al. 1999).

The accumulation of a substantial GRB population by BATSE shows that they are isotropically distributed. The simplest explanation for this fact is the GRB cosmological origin, at variance with pre-CGRO view in which GRBs were associated to neutron stars distributed in a thick galactic disk.

The GRB cosmological origin has been clamorously confirmed more recently by the Beppo-SAX observations (Costa et al. 1997) of counterparts in the X-ray band of some GRBs. Thanks to these observations, it has been possible not only a X-ray identification of GRBs, but also the determination with a better accuracy of the GRB source position, allowing the consequent tracking of optical and radio telescopes (Galama et al. 1997).

In turn, redshift measurements (through optical observations) allow to evaluate the distance of some GRBs and therefore to derive the amount of energy they should have radiated in an isotropic explosion (henceforth indicated as $\mathcal{E}_\gamma^{iso}$) in the soft $\gamma$-ray energy band.

Currently, the most popular explanation for the GRB phenomenon is the fireball model (Rees & Mészáros 1992), i. e. the dissipation of the kinetic energy of a relativistic (with Lorentz factor $\Gamma \sim 10^2$–$10^3$) expanding blast wave in internal shocks (see Piran 1999 for a recent review). Due to the short time scale variability of GRBs ($\gtrsim 10^{-3}$ s), soft $\gamma$-rays are generally considered to be emitted by relativistic electrons, through synchrotron and inverse Compton mechanisms. This model is particularly successful in explaining the long wavelength afterglow behaviour observed for some GRBs.

In Table 1, for some bursts for which it has been possible to estimate the distance, we give their redshift $z$ and the inferred $\mathcal{E}_\gamma^{iso}$ values. Note that if GRBs are beamed sources as indicated by afterglow observations (Huang et al. 1999), the emitted energy would be decreased by the factor $\Delta\Omega/4\pi$, where $\Delta\Omega$ is the beaming angle. As one can see in Table 1, the brightest burst

**Table 1.** For some bursts for which it has been possible to estimate the distance, we give their redshift $z$ and the energy $\mathcal{E}_\gamma^{iso}$ radiated in the soft $\gamma$-ray band. In the third column we indicate how the GRB redshift has been measured: (a) from the redshift of the host galaxy; (b) from Lyman break of the optical afterglow; (c) from absorption lines in the optical afterglow.

| GRB | $z$ | Note | $\mathcal{E}_\gamma^{iso}$(erg) | Ref. |
|---|---|---|---|---|
| 970228 | 0.695 | a | $5.2 \times 10^{51}$ | Djorgovski et al. 1999a |
| 970508 | 0.835 | c | $\sim 7 \times 10^{51}$ | Metzger et al. 1997 |
| 971214 | 3.42 | a | $\sim 3 \times 10^{53}$ | Kulkarni et al. 1998 |
| 980329 | $\sim$5 | b | $\gtrsim 10^{54}$ | Fruchter 1999 |
| 980613 | 1.0964 | a | $5.2 \times 10^{51}$ | Djorgovski et al. 1999b |
| 980703 | 0.966 | a | $\gtrsim 10^{53}$ | Djorgovski et al. 1998 |
| 990123 | $\gtrsim 1.6$ | c | $\gtrsim 3 \times 10^{54}$ | Kulkarni et al. 1999 |
| 990510 | 1.62 | c | $2.9 \times 10^{53}$ | Harrison et al. 1999 |
| 991208 | 0.7055 | c | $1.03 \times 10^{53}$ | Sagar et al. 2000 |
| 991216 | 1.02 | a | $6.7 \times 10^{53}$ | Sagar 2000 |

*Send offprint requests to*: G. Ingrosso

(GRB 990123) has $\mathcal{E}_\gamma^{iso} \gtrsim 3 \times 10^{54}$ erg showing that in a GRB event up to one solar mass can be radiated in form of soft $\gamma$-rays.

It is also well known that GRBs are sources of high-energy $\gamma$-rays, as it has been shown by the EGRET spark chamber, which detected $\gamma$-rays in the energy band $\sim 30$ MeV - 20 GeV, from a high percentage of bright BATSE bursts (Schneid et al. 1992, 1995 and Hurley et al. 1994). These observations clearly show that the GRB phenomenon is not exclusively the domain of the soft $\gamma$-ray energy band.

The natural question which raises is the production mechanism of the high-energy $\gamma$-rays (with energy $E_\gamma \geq 1$ GeV) that, in principle, may be due to both electrons and protons.

However, if the electron emission spectra which fit BATSE observations are extrapolated in the high-energy domain, the obtained photon fluxes at Earth are well below the values detected by EGRET (Pilla & Loeb 1998). This fact manifestly implies that high-energy $\gamma$-rays from GRBs cannot be entirely accounted for by radiation emitted by accelerated electrons.

Indeed, as is usual for many high-energy astrophysical sources (such as AGN, Seyfert galaxies, etc.), also for GRBs it is expected that the most efficient mechanism to produce high-energy $\gamma$-rays is via $\pi^0$ decay of pions primarily produced through proton-nucleon ($pN$) interactions.[1]

Within the framework of the fireball model for GRBs, it has been recently argued that all GRB events could release roughly the same amount of energy $\mathcal{E} \sim 10^{54} \Delta\Omega$ erg (Totani 1999).[2]

The total GRB energy is shared between electrons and protons which, at least in the initial stage of internal shock generation, carry a much larger amount of energy than electrons, by a factor $m_p/m_e \sim 2000$.

It is uncertain what fraction of the initial energy is subsequently transferred by protons to electrons, but the simplest Coulomb interaction cannot be very efficient within the shortest GRB time-scale variability of $\simeq 10^{-3}$ s. Another mechanism to transfer energy to electrons could be through proton synchrotron emission and subsequent annihilation $\gamma\gamma \to e^+e^-$, but also this process is generally inefficient owing to its quite long time-scale compared with the GRB variability.[3]

Indeed, according to the fireball model, the energy transfer from the proton into the electron component occurs via internal shock generation. The efficiency of this mechanism depends sensitively on the fireball Lorentz factor $\Gamma$ so that the spread of the $\Gamma$ values should account for the spread in the observed soft $\gamma$-ray emissivity $\mathcal{E}_\gamma$ of the electronic component.

However, as one can see from Table 1 at least for the few GRBs for which it has been possible to estimate the distance, the energy $\mathcal{E}_\gamma^{iso}$ is a minor fraction (between $\sim 10^{-4}$ and $\sim 0.1$) of the total GRB energetic assumed by Totani (1999). So, it is likely that a substantial fraction of $\mathcal{E}$ remains in form of accelerated protons coming out from the GRB source with a total energy $\mathcal{E}_p \simeq 10^{54} \Delta\Omega$ erg. This is the reference value that we will adopt in our calculations.

It is by now widely recognised that GRBs accelerate protons at energies even up $\sim 10^{20}$ eV (Waxman 1995, Vietri 1995, Böttcher & Dermer 1998). If it is so, these protons could in turn interact with nucleons in the medium surrounding the GRB source, giving rise to $\pi^0$ and ultimately to a high-energy $\gamma$-ray flux on Earth. Clearly, a key requirement of this model is the existence of a dense enough cloud (which serves as a target for $pN$ interactions) surrounding the GRB source or, alternatively, the existence of a cloud along the line of sight observer-burst and close enough to the source. Moreover, as we shall see in the following sections, in order to have an observable high-energy $\gamma$-ray flux on Earth, the cloud number density $n_N$ has to be in the range $10^8 - 10^{11}$ cm$^{-3}$.

At first sight, so high densities may seem unlikely. However, the presence of high density regions nearby GRB sources has been invoked in several cases. For example, Katz 1994 has shown that a cloud with density $n_N \sim 2 \times 10^{11}$ cm$^{-3}$ and size $r_0 \sim 10^{15}$ cm is required to explain the delayed high-energy photons observed more than an hour following the GRB 940217. Moreover, Piro et al. (1999) and Yoshida et al. (1999) have reported an iron emission line in the X-ray afterglow spectrum of GRB 970508 and of GRB 970828. The obtained line intensity requires a medium of density $n_N \simeq 10^{10}$ cm$^{-3}$, thickness $\Delta R \simeq 10^{14}$ cm and size $10^{16}$ cm (Lazzati et al. 1999). The involved geometry of the target region could be either a cloud with a significant covering factor located off the line of sight burst-observer or a homogeneous spherical shell centered in the GRB progenitor.

Three main classes of models have been proposed for the origin of GRBs: neutron star-neutron stars (NS-NS) mergers (Paczynski 1986 and Eichler et al. 1989), "hypernovae" or failed type Ib supernovae (Woosley 1993 and Paczynski 1998) and "supranovae" (Vietri & Stella 1998). In the NS-NS model the target cloud could be associated to an accretion disk around the GRB source. In the hypernova case, the burst is caused by the evolution of a massive ($\simeq 100\ M_\odot$) star located in a dense molecular cloud, while in the supranova scenario, a shell-like

[1] In principle, accelerated protons could radiate their energy through synchrotron emission, before strong interactions are in operation. However, synchrotron emission is relevant only for protons with extremely high-energy $\sim 10^{20}$ eV (Vietri 1997) and it is negligible for the production of $\sim 1$ GeV - 10 TeV photons, which are produced much more efficiently through $pN$ interactions.

[2] We would like to mention that Kulkarni et al. (2000) have suggested that afterglow observations may offer a robust method to evaluate the GRB energetics. In particular, from late time X-ray observations and assuming that the fraction of shock energy carried by electrons is close to equipartition, Freedman & Waxman (1999) estimate the GRB energy release $\mathcal{E}$ to be in the range $3 \times 10^{51} - 3 \times 10^{53}$ erg, which must be considered a more conservative range of (low) GRB energetics. However, both the Totani (1999) and the Freedman & Waxman (1999) estimates for $\mathcal{E}$ may still be considered consistent with observations, due to the uncertainties and precarious nature of GRB energy estimates (see also Kulkarni et al. 2000).

[3] It has been shown that the proton cooling time becomes comparable to the GRB duration only at the maximum proton energy ($\sim 10^{20}$ eV), and, even in this case, the energy radiated in the GeV-TeV range is considerable only if the proton energy spectrum is harder than the typical shock acceleration spectrum $J_p(E_p) \propto E_p^{-2.2}$ (Totani 1998a, 1998b).

supernova remnant is naturally left over around the location of the GRB.

In all the above mentioned scenarios, high-energy $\gamma$-ray production via $pN$ interactions is expected with an intensity roughly proportional to $n_N$. Moreover, a prediction of our model is that a long wavelength afterglow emission from GRBs should be present only if the cloud covering factor is low enough.

A feature of the model in question is a delay in the arrival times of the high-energy $\gamma$-rays with respect to the soft $\gamma$-rays and a temporal spread of the signal, as a consequence of the proton deflection due to the presence of magnetic fields in the region surrounding the GRB source. A lower limit to the magnetic field is surely the typical interstellar magnetic field $B_{ISM} \simeq 1\ \mu$G.

The aim of the paper is to estimate in detail the flux on Earth of $\gamma$-rays in the GeV-TeV energy range from cosmological GRBs and in particular the temporal structure of the signal. In Sects. 2 and 3 we present the model we use to calculate the source function for $\gamma$-ray production via $pN$ interactions. In Sect. 4 we present our results for the $\gamma$-ray flux on Earth, taking into account the intergalactic $\gamma$-ray absorption. In Sect. 5 we briefly discuss the ground-based high-energy $\gamma$-ray experiments in connection with GRB observations and give the model parameter range for which the GRB high-energy detection may be possible by the ARGO-YBJ experiment (Abbrescia 1996, Bacci 1998). Finally, our conclusions are presented in Sect. 6.

## 2. The model

As previously stated, we assume that the GRB source emits an amount of energy $\mathcal{E}_p \sim 10^{54}\Delta\Omega$ erg in the form of relativistic protons, released during a time $\Delta t \sim 1$ s, at a distance $r_0 \sim 10^{16}$ cm from the central GRB source[4]. We further assume that there exists a dense enough cloud near/around the GRB source so that accelerated protons subsequently interact with nucleons in the cloud giving rise to $\pi^0$ and ultimately to high-energy $\gamma$-rays.

An essential ingredient to calculate the $\gamma$-ray production rate is the proton flux $J_p(E_p, r)$ which is a function of both the proton energy and the radial coordinate $r$. As implied by Fermi type shock acceleration models (see e.g. Gaisser 1990, Berezinskii et al. 1990), $J_p(E_p, r)$ is assumed to follow a power-law energy spectrum. It moreover depends on the distance $r$ from the central engine according to a function $f(r)$ to be later specified

$$J_p(E_p, r) = C(E_p/\mathrm{GeV})^{-a_p} f(r) \quad \mathrm{protons\ cm^{-2}\ s^{-1}\ sr^{-1}\ GeV^{-1}}\ . \tag{1}$$

Assuming $f(r_0) = 1$, the constant $C$ is determined by the normalization condition which yields

$$C = \frac{1}{4\pi r_0^2}\frac{1}{\mathcal{I}(a_p)}\frac{\mathcal{E}_p}{\Delta t} \tag{2}$$

where

$$\mathcal{I}(a_p) = \int_{E_0}^{+\infty} (E_p/\mathrm{GeV})^{-a_p} E_p dE_p\ , \tag{3}$$

and $E_0 = \Gamma m_p c^2$ is the minimum proton energy.

As far as the value of the energy spectral index $a_p$ is concerned, since protons are accelerated by shock waves moving with ultrarelativistic velocities and further diffusive processes are negligible during the time before $pN$ interactions, we will adopt the relevant value $a_p \simeq 2.2$ (Bednarz & Ostrowski 1998, Vietri 2000).[5]

The radial profile $f(r)$ depends of course on the geometrical dilution factor which follows the $r^{-2}$ dependence. Moreover, we take into account that protons emerging from the GRB source at the distance $r_0$, subsequently contribute to the production of high-energy $\gamma$-rays just in their first $pN$ interaction (for simplicity we neglect interactions of secondary particles with lower energy). The probability that this first interaction occurs after a path of length $l$ is equal to $\exp(-\sigma_{pN} n_N l)$, where $\sigma_{pN}$ is the total $pN$ cross-section ($\sigma_{pN} \sim 3 \times 10^{-26}\,\mathrm{cm}^2$, nearly independent of the proton energy) and $n_N$ is the nucleon number density of the cloud. Correspondingly, the average length travelled by protons in the surrounding medium results to be $\Delta R = (\sigma_{pN} n_N)^{-1} \simeq 10^{-3}$ pc $(10^{10}\ \mathrm{cm^{-3}}/n_N)$. The mass enclosed will be $M_{\mathrm{cl}} \sim 0.4\ M_\odot (r_0/10^{15}\ \mathrm{cm})^2$ in a shell-like cloud geometry and $M_{\mathrm{cl}} \sim 0.2\ M_\odot (10^{10}\ \mathrm{cm^{-3}}/n_N)^2$ in the case of an intervening cloud.

An important point to stress is that high-energy $\gamma$-rays may in principle be re-absorbed if the path they have to travel inside the cloud (after being produced) is long enough. If the dominant absorption process is through $\gamma H$ interactions, the corresponding column density is $\simeq 3 \times 10^{25}\ \mathrm{cm^{-2}}$ (Particle Data Group 1996) or, equivalently, an attenuation length $l_{\gamma H} \sim \Delta R$. In this case high-energy $\gamma$-rays should suffer attenuation. However, it is expected that clouds nearby the GRB source present a high ionization degree, so that the relevant absorption processes are $\gamma e$ and $\gamma p$ interactions, which have a much smaller cross-section implying a large $\gamma$ free-path before re-absorption.

Another effect we have to consider in defining the function $f(r)$ is the deflection of the proton trajectory before the interaction with target nucleons occurs. In fact, protons are deflected by the intervening magnetic field $B$ by an angle $\alpha(E_p) = l/R_L(E_p)$, where $R_L(E_p) = E_p/(eB)$ is the Larmor radius. From simple geometrical considerations, protons starting at $r = r_0$ and reaching the radial coordinate $r$ are deflected by an angle

$$\alpha \simeq \arcsin\left(\frac{r - r_0}{R_L(E_p)}\right)\ , \tag{4}$$

so that $l$ is given by

[4] We have verified that our results do not sensitively depend on the adopted values of $\Delta t$ and $r_0$.

[5] In this respect we mention that the observed local CR spectrum has a power index $a_p \simeq 2.75$, softer than the previous one. As it is well known, this is due to the fact that CRs diffuse throughout the Galaxy, scattering on the hynomogeneities of the magnetic field. In this diffusion process, high-energy particles rapidly loose energy and at the end of the diffusion process, the CR power index gets increased with respect to initial value.

$$l(E_p, r) \simeq R_L(E_p)\ \arcsin\left(\frac{r - r_0}{R_L(E_p)}\right) \tag{5}$$

Moreover, protons deflected by an angle $\alpha > \pi/2$, i.e. protons that have travelled for a length $l > \pi R_L(E_p)/2$, turn back towards the GRB source, so they presumably do not contribute to the production of observable high-energy $\gamma$-rays.

On the basis of these assumptions, the radial profile takes the form:

$$\begin{aligned} f(r) &= \left(\frac{r_0}{r}\right)^2 \exp[-\sigma_{pN} n_N l(E_p, r)] \quad \text{if } l < R_L(E_p) \\ f(r) &= 0 \qquad\qquad\qquad\quad \text{if } l > R_L(E_p)\ . \end{aligned} \tag{6}$$

The effect of the presence of a magnetic field around the GRB source is particularly relevant as regards the $\gamma$-ray production rate. The ratio $\eta = R_L(E_p)\sigma_{pN} n_N$ between the scale length for proton deflection by magnetic fields $R_L(E_p)$ and that for $pN$ interactions $(\sigma_{pN} n_N)^{-1}$, sets the relative strength of the two effects, the deflection and the interaction.

In the case $\eta \lesssim 1$, protons can be significantly deflected before interacting, so that most of the generated $\gamma$-rays will not reach Earth. Now, since $R_L \propto E_p$, once $n_N$ and $B$ are given, the condition $\eta \lesssim 1$ means

$$E_p \lesssim 10^3\ \mathrm{GeV} \left(\frac{10^{10}\ \mathrm{cm}^{-3}}{n_N}\right)\left(\frac{B}{1\ \mu\mathrm{G}}\right)\ , \tag{7}$$

where the magnetic field at $r > r_0$ has been taken of the order of magnitude of the interstellar magnetic field.

## 3. Source function

As we discussed in the Introduction the relevant mechanism for the high-energy $\gamma$-ray production with $E_\gamma > 1$ GeV is the process

$$pN \rightarrow\ \pi^0 + \text{ anything}\ ,\ \ \pi^0\ \rightarrow\ \gamma\gamma\ . \tag{8}$$

Following Dermer 1986, the production spectrum of high-energy $\gamma$-rays resulting from $pN$ collisions is given by

$$\begin{aligned} q_\gamma(E_\gamma, r) = 16\pi^2 n_N \int_{E_\pi^{min}}^{+\infty} dE_\pi \int_{E_0}^{+\infty} dE_p\ J_p(E_p, r) \times \\ \int_{cos\theta_{max}}^{1} dcos\theta\ E^* \frac{d^3\sigma^*}{dp^{*3}} \quad \gamma\ \mathrm{cm}^{-3}\ \mathrm{s}^{-1}\ \mathrm{GeV}^{-1} \end{aligned} \tag{9}$$

where $\theta$ is the angle between the line of sight and the proton direction and asterisks refer to CM frame. Provided $-1 \leq \cos\theta_{max} \leq 1$, one gets $\cos\theta_{max} = \Gamma E_\pi - E^*_{max}/(\beta\Gamma p_\pi)$.

According to Stephens-Badhwar's model (Stephens & Badhwar et al. 1981), the Lorentz invariant cross-section for $\pi^0$ production in $pN$ collisions inferred from high-energy experimental data can be parameterized in the form

$$E^* \frac{d^3\sigma^*}{dp^{*3}} = A e^{-Bp_\perp}(1 - \tilde{x})^{C_1 - C_2 p_\perp + C_3 p_\perp^2} \tag{10}$$

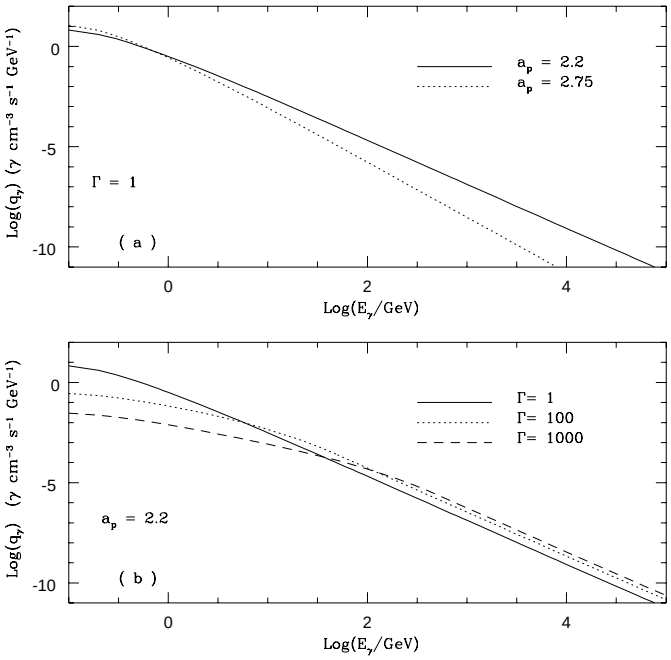


**Fig. 1a and b.** Production spectra $q_\gamma(E_\gamma)$ of high-energy $\gamma$-rays are given as a function of $E_\gamma$ for several values of $\Gamma$ and $a_p$, assuming $n_N = 10^9\,\mathrm{cm}^{-3}$, and $C = 10^{23}/(4\pi\mathcal{I}(a_p))$ protons cm$^{-2}$ s$^{-1}$ sr$^{-1}$ GeV$^{-1}$. In **a**, we set $\Gamma = 1$ and give results for $a_p = 2.2$ (full line) and 2.75 (dotted line). In **b**, for the relevant value $a_p = 2.2$, we see the effect on $q_\gamma(E_\gamma)$ of increasing the values of $\Gamma = 1$, 100, 1000.

where $\tilde{x} = (x^{*2}_\parallel + (4/s)(p^2_\perp + m^2_\pi))^{1/2}$, $x^*_\parallel = p^*_\parallel/p^*_{max}$, $s = 2m_p(E_p + m_p)$ and $A = 140$, $B = 5.43$, $C_1 = 6.1$, $C_2 = 3.3$, $C_3 = 0.6$.

Numerical values of the $\gamma$-ray source function in Eq. (9) depend on the proton flux $J_p(E_p, r)$ at distance $r$, the Lorentz factor $\Gamma$ and the nucleon number density $n_N$. The proton flux, in turn, depends on the constant $C$ and the spectral index $a_p$.

In order to clarify the dependence of $q_\gamma(E_\gamma, r)$ on the relevant parameters $a_p$ and $\Gamma$ we assume, as reference values, $n_N \simeq 10^9\,\mathrm{cm}^{-3}$ and $C \simeq 10^{23}/(4\pi\mathcal{I}(a_p))$ protons cm$^{-2}$ s$^{-1}$ sr$^{-1}$ GeV$^{-1}$ or, equivalently form Eq. (2), $r_0 \simeq 10^{16}$ cm, $\mathcal{E}_p \simeq 10^{54}\Delta\Omega$ erg and $\Delta t \simeq 1$ s.

In Figs. 1a and 1b we give $q_\gamma(E_\gamma)$ as a function of $E_\gamma$. In Fig. 1a $\Gamma$ is fixed to be one, while $a_p$ is 2.2 (continuous line) and 2.75 (dotted line). In Fig. 1b we set $a_p = 2.2$, while $\Gamma$ values are 1, 100 and 1000. As we can see in Fig. 1a, consideration of a harder proton spectrum increases the high-energy $\gamma$-ray production rate (by a factor of $\sim 100$ at $E_\gamma \simeq 1$ TeV). Moreover, we find that the $\gamma$-ray spectrum roughly follows a power law behaviour $q_\gamma(E_\gamma, r) \sim E_\gamma^{-a_\gamma}$, with power index $a_\gamma \simeq a_p$. In Fig. 1b, we see that an enhanced high-energy $\gamma$-ray production is also obtained by increasing the $\Gamma$ values.

Production spectra for different values of $\tilde{C}$ and $\tilde{n}_N$ can be obtained from the results in Fig. 1 by multiplying the quoted values by the factor $\tilde{C}\ (4\pi\mathcal{I}(a_p))/10^{23}) \times \tilde{n}_N/10^9$. In particular, assuming $\tilde{n}_N = 1\,\mathrm{cm}^{-3}$ and $\tilde{C} = 2.1$ protons cm$^{-2}$ s$^{-1}$ sr$^{-1}$ GeV$^{-1}$ we can verify that our calculations reproduce, within

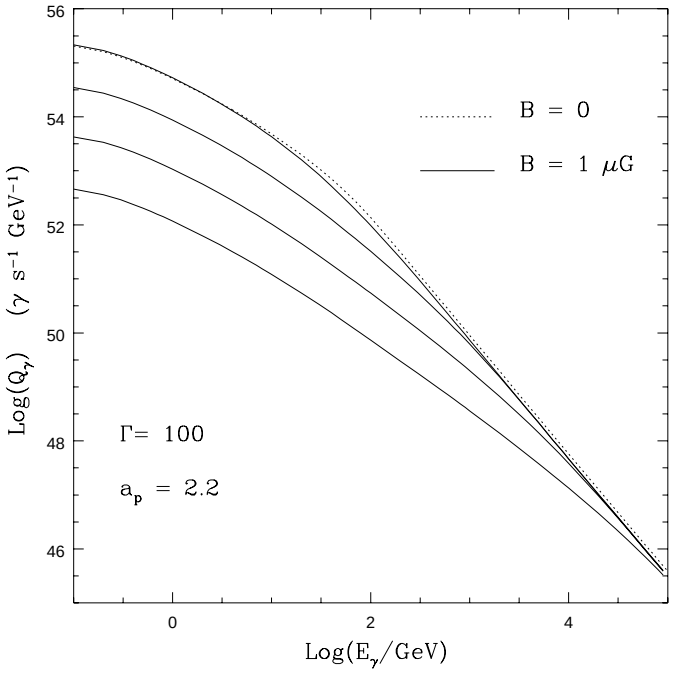


**Fig. 2.** The differential high-energy $\gamma$-ray luminosity emitted by a GRB source via pN interactions is given as a function of $E_\gamma$, for $B = 0$ (dotted line) and $B = 1$ $\mu$ G (continuous lines). In the latter case, the cloud density values are $n_N = 10^8,\ 10^9,\ 10^{10},\ 10^{11}$ cm$^{-3}$, from the bottom to the top. Values of $Q_\gamma$ for different model parameters, can be obtained by using the scaling relation $Q_\gamma(\mathcal{E}_p^{iso}/10^{55}\ \mathrm{erg})(\Delta t/1\mathrm{s})^{-1}$.

a few percent, the results on the $\gamma$-ray spectrum produced by the local cosmic-ray interactions with the interstellar medium (Mori 1997).

## 4. Gamma-ray flux on Earth

In order to calculate the differential $\gamma$-ray luminosity $Q_\gamma(E_\gamma; r_0, R)$, we have to integrate the source function $q_\gamma(E_\gamma, r)$ in Eq. (9) over the whole volume of the region in which the $pN$ interactions occur, i.e. the shell between the radii $r_0$ and $R \simeq r_0 + 1/(\sigma_{pN} n_N)$:

$$Q_\gamma(E_\gamma; r_0, R) = \int_{r_0}^{R} q_\gamma(E_\gamma, r) r^2 dr \ \ \gamma\ \mathrm{s}^{-1}\ \mathrm{GeV}^{-1}\ . \qquad (11)$$

Note that here, as stated at the end of Sect. 2, we have neglected re-absorption of the $\gamma$-rays in the cloud itself.

The explicit dependence of $Q_\gamma(E_\gamma; r_0, R)$ on the GRB parameters is obtained by using Eq. (1) in Eq. (9), namely

$$Q_\gamma(E_\gamma; r_0, R) = \frac{4\pi n_N \mathcal{E}_p}{\mathcal{I}(a_p)\Delta t} \int_{E_\pi^{min}}^{+\infty} dE_\pi \int_{E_p^0}^{+\infty} E_p^{-a_p} dE_p \times$$
$$\int_{r_0}^{R} dr\ \exp[-\sigma_{pN} n_N l(E_p, r)] \int_{cos\theta_{max}}^{1} dcos\theta\ E^* \frac{d^3\sigma^*}{dp^{*3}}\ . \qquad (12)$$

As we pointed out in Sect. 2, the presence of magnetic fields around the GRB source affects the differential $\gamma$-ray luminosity in Eq. (12) through the term $l(E_p, r)$. In Fig. 2, adopting the same values for the GRB parameters as in Fig. 1 and further assuming $a_p = 2.2, \Gamma = 100$ and $n_N$ in the range $10^8$–$10^{11}$ cm$^{-3}$, we compare $Q_\gamma(E_\gamma)$ obtained in the case $B = 0$ (in which protons follow straight trajectories) with the case $B = 1$ $\mu$G (in which protons of lower energies are deflected). As one can see, in the case $B = 0$, one obtains the same curve for any value of the cloud number density. This result is expected since, increasing the density, the scale length for the $pN$ interactions decreases, but the projected column density $Rn_N$ remains constant.

From Fig. 2 one can see that the effect of the presence of the magnetic fields is to diminish the $\gamma$-ray production rate, in the sense that for a given value of $B$, $Q_\gamma(E_\gamma; r_0, R)$ decreases as $n_N$ decreases. In fact, low energy photons are mainly generated by $pN$ interactions of low energy protons (generally with energies of one order of magnitude above the photon energy), which are more easily deflected by the intervening magnetic fields and therefore give rise to photons that cannot reach the observer. There exists, however, a limiting density ($\simeq 10^{11}$ cm$^{-3}$ in the case $B \simeq 1$ $\mu$G) above which most of the protons interact before suffer substantial deflection so that the differential $\gamma$-ray luminosity for $B = 0$ is recovered.

Another important effect of the presence of magnetic fields is a temporal spread of the emitted high-energy $\gamma$-ray signal on Earth. To better analyze this point, we can assume a proton injection time $\Delta t \simeq 1$ s, which may be considered instantaneous since it is much smaller than the average proton interaction time $(\sigma_{pN} n_N c)^{-1} \simeq 10^5\,\mathrm{s}\,(10^{10}\,\mathrm{cm}^{-3}/n_N)$. Accordingly, denoting by $t_0$ the instant at which photons arrive on Earth in the case $B = 0$ (no proton deflection), the delay $t - t_0$ is a function of the length $l$ travelled by the protons (before interacting) and of the deflection angle $\alpha$ given by Eq. (4). So we get

$$t_i - t_0 = \frac{R_L(E_p)}{c} \left( \arcsin \frac{r_i - r_0}{R_L(E_p)} - \frac{r_i - r_0}{R_L(E_p)} \right) \qquad (13)$$

Vice versa, one can say that photons with time delay between $t_1$ and $t_2$ are produced by protons of energy $E_p$ only if these protons have interacted in the shell $r_1(E_p) - r_2(E_p)$. Here $r_i(E_p) \equiv r(t_i, E_p)$, and $r_i$ and $t_i$ are related by Eq. (13).

We note that the relation above in Eq. (13) allows to estimate the time duration $T_{HE}$ of the high-energy GRB signal. If $\eta \ll 1$, namely the proton deflection is substantial before $pN$ interactions take place, one gets $T_{HE} \simeq R_L(E_p)c^{-1} \simeq 10^3$ s $(E_p/\mathrm{GeV})$. In other words, if one observe photons with energy $E_\gamma \simeq 100$ GeV (which are mainly produced by protons with $E_p \simeq 1$ TeV) the expected GRB duration at that energy is $\simeq 10$ days. If protons do not suffer strong deflection before interacting, i.e. $\eta \gg 1$, one obtains $T_{HE} \simeq R_L(E_p)c^{-1}\eta^{-3}$. This implies that the high-energy GRB duration may become shorter and then more advantageous in a observational perspective.

As next, let us estimate the differential $\gamma$-ray fluence on Earth $F_\gamma(E_\gamma; t_i, t_j)$, during the time interval $t_i - t_j$. To this aim, we calculate $Q_\gamma(E_\gamma; t_i, t_j)$ relative to photons with arrival time between $t_i$ and $t_j$, by substituting $r_0$ and $R$ with $r_i$ and $r_j$ in Eq. (12) respectively. So:

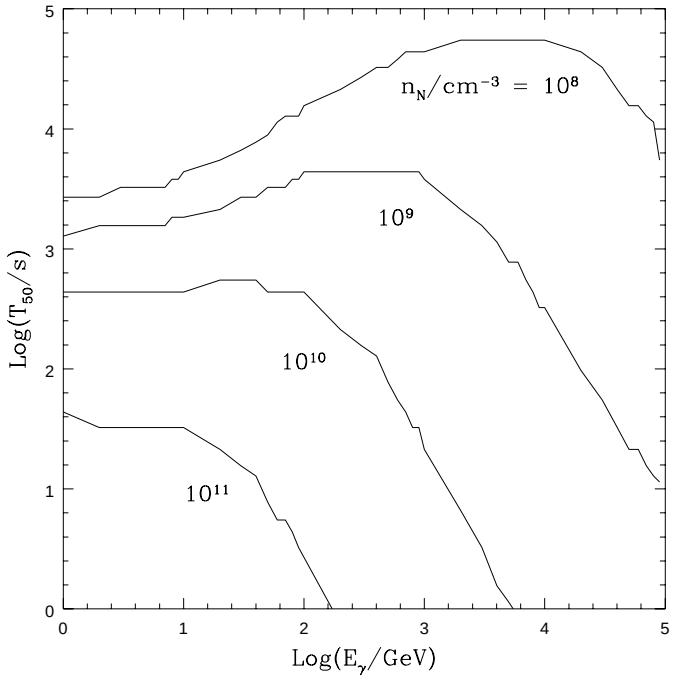


**Fig. 3.** The duration time $T_{50}$ is given as a function of $E_\gamma$ for selected values of the cloud density $n_N = 10^8,\ 10^9,\ 10^{10},\ 10^{11}\,\mathrm{cm}^{-3}$.

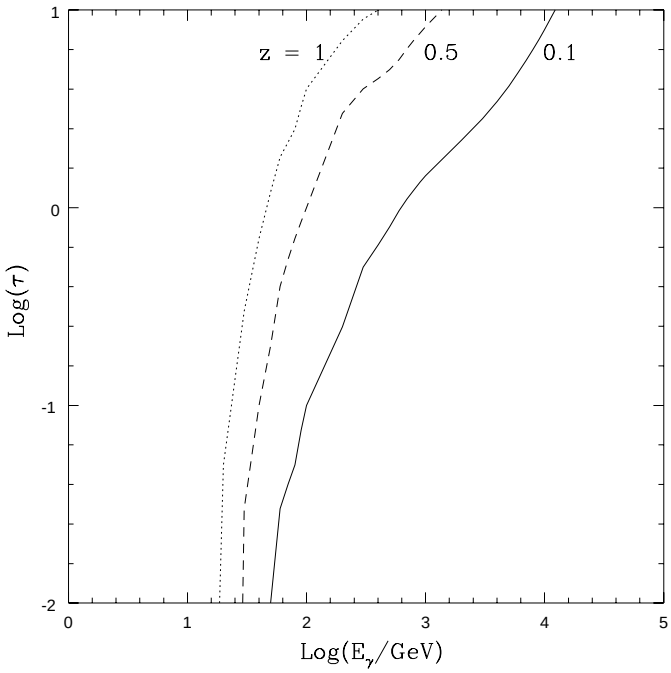


**Fig. 4.** The optical depth $\tau$ for high-energy $\gamma$-ray interactions with background low-energy photons is given as a function of the energy $E_\gamma$, for selected values of the source redshift $z = 0.1$, 0.5, 1.

$$F_\gamma(E_\gamma; t_i, t_j) = \frac{Q_\gamma(E_\gamma(1+z); t_i, t_j)\Delta t(1+z)}{4\pi D_L^2(z)} \qquad (14)$$

$$\gamma\ \mathrm{cm}^{-2}\ \mathrm{GeV}^{-1}\ ,$$

where $\Delta t$ is the proton injection time and

$$D_L(z) \simeq \frac{c}{H_0}\left(z + \frac{1}{2}(1-q_0)z^2\right), \qquad (15)$$

is the GRB luminosity distance, with $H_0 \simeq 70$ Km s$^{-1}$ Mpc$^{-1}$ and $q_0 \simeq 0.15$. Clearly, the differential $\gamma$-ray flux on Earth at the time $t_i$ can be evaluated by $\Phi_\gamma(E_\gamma; t_i) = F_\gamma(E_\gamma; t_i, t_i+dt)/dt$.

We note that by substituting Eq. (12) into Eq. (14) the injection time $\Delta t$ cancels out, so that it does not affect the $\gamma$-ray signal on Earth, provided the observational time is $> \Delta t$.

It is interesting and important in connection with the observability at high-energy of GRB events, to study in more details the temporal behaviour of the high-energy $\gamma$-ray flux arriving on Earth. To this purpose, in analogy to the GRB soft $\gamma$-ray observations, we define the time $T_{50}(E_\gamma)$ needed to receive on Earth the 50% of the total number of photons of energy $E_\gamma$. In Fig. 3 we show $T_{50}$ as a function of the photon energy, for different values of the cloud density $n_N$. As one can see, for each density value, there exist a limiting value of $E_\gamma$ above which $T_{50}$ decreases with increasing the photon energy. Moreover, $T_{50}$ rapidly decreases as $n_N$ increases, for a given value of $E_\gamma$. From the same figure and the discussion above, it is clear that the higher is $n_N$, more easily the source is observable at high energy. This is essentially due to two reasons: the flux $\Phi_\gamma$ depends approximately linearly on $n_N$ and $T_{50}$ is shorter as $n_N$ increases. It is also obvious that, in order to accumulate a significant amount of $\gamma$-ray photons, high-energy observations must last substantially longer if the cloud density $n_N$ is rather low.

As we stated in Sect. 1, it is nowadays widely recognized that GRBs are cosmological sources. In this case high-energy $\gamma$-rays suffer attenuation (by electron-positron pair creation) due to their interaction with photons of the intergalactic infrared radiation field (IIRF). This effect is taken into account through the absorption coefficient $\tau(E_\gamma, z)$, which can be evaluated through the observational data on the IIRF and adopting theoretical models of the galactic spectral energy distribution of the IIRF from stars and dust reradiation (Stecker & De Jager 1997, Salomon & Stecker 1998). In Fig. 4, for illustrative purposes, we plot $\tau$ as a function of $E_\gamma$, for some values of the source redshift $z$. As one can see, for GRB sources at $z > 0.5$, photons with energy $E_\gamma \gtrsim 100$ GeV are heavily absorbed, while for closer GRBs with $z \lesssim 0.1$ photons with $E_\gamma \lesssim 1$ TeV survive absorption. So, the differential $\gamma$-ray fluence observed at Earth will be

$$F_\gamma^\oplus(E_\gamma; t_i, t_j) = F_\gamma(E_\gamma; t_i, t_j)\exp[-\tau(E_\gamma, z)]\ . \qquad (16)$$

An analogous relation allows us to calculate the differential $\gamma$-ray flux on Earth $\Phi_\gamma^\oplus(E_\gamma; t)$. In Figs. 5a and 5b, $\Phi_\gamma^\oplus$ at different arrival times is given as a function of the photon energy, for GRB sources at $z = 0.1$ and $z = 0.5$, respectively.

In Fig. 6, for the same values of the source redshift $z$, the differential fluence on Earth is given in different time intervals. As one can see in Figs. 5 and 6, due to the presence of magnetic fields, GRBs may last much longer in the high-energy band than in the soft $\gamma$-ray band.

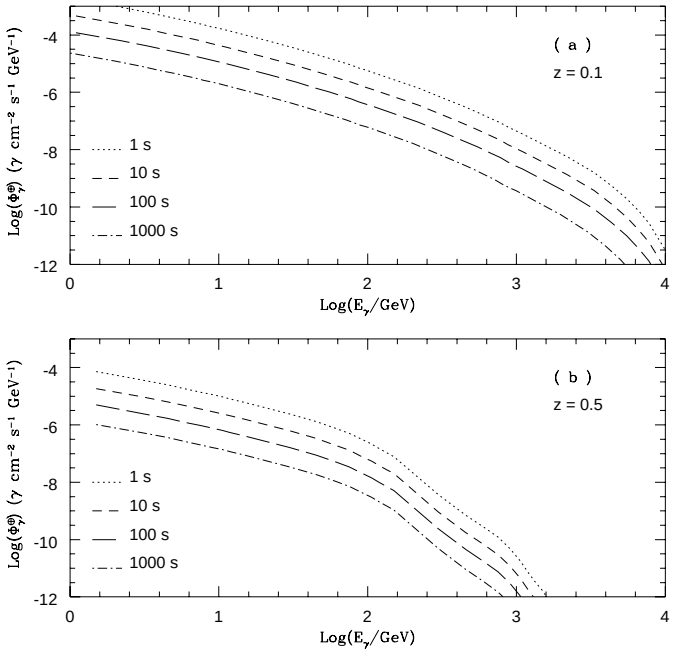


**Fig. 5a and b.** Differential high-energy $\gamma$-ray fluxes on Earth are given at different time $t_i = 1,\ 10,\ 100,\ 1000$ s. The GRB source redshift is fixed at the value $z = 0.1$ **a** and $z = 0.5$ **b**.

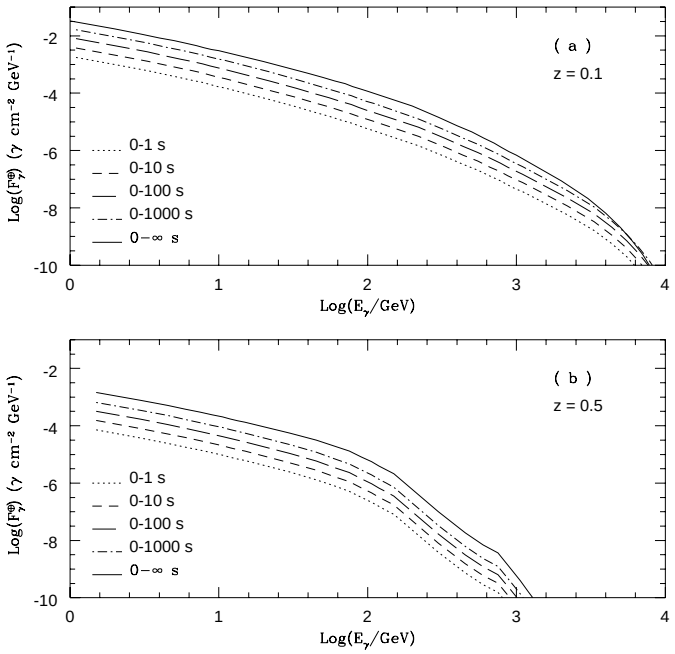


**Fig. 6a and b.** Differential high-energy $\gamma$-ray fluences on Earth are given for different time intervals $(t_i, t_j)$ = (0-1), (0-10), (0-100), (0-1000), (0,$\infty$) s. As in Figs. 5a and 5b, the GRB redshift is fixed to be $z = 0.1$ **a** and $z = 0.5$ **b**.

## 5. Ground-based high-energy gamma-ray experiments

Nowadays, the possibility to detect GRBs in the GeV-TeV energy range relies essentially on ground-based experiments (see e.g. Vernetto 2000). Less constrained in size than space born detectors, they can explore high-energy $\gamma$-rays detecting the secondary particles generated by their interaction in the atmosphere: Cherenkov photons in the case of Cherenkov telescopes as HEGRA AIROBICC (Padilla et al. 1998), Milagrito (McEnery et al. 1999) and Whipple (Connaughton et al. 1997) or $e^{\pm}$ in the case of extensive air shower array experiments as the Tibet air shower array (Amenomori et al. 1996) and the planned detector ARGO (Abbrescia 1996, Bacci 1998).

The Tibet shower array and the HEGRA AIROBICC experiment have independently reported significant excesses of 10–20 TeV $\gamma$-rays in coincidence with a few GRBs.

In particular, among the 57 GRBs detected by BATSE (Meegan et al. 1996) in the field of view of the Tibet array, some of them show a significant excess of 10 TeV $\gamma$-ray events with a timescale of $\sim 10$ s. The statistical significance was estimated to be about 6 $\sigma$.

There are four GRBs in the field of view of HEGRA array, and the HEGRA group observed 11 $\gamma$-ray-like events above 20 TeV in a minute bin coincident with GRB 920925c in the GRANAT/WATCH GRB catalog (Sazonov et al. 1998), whereas only 0.93 events are expected as background (the statistical significance is therefore 5.4 $\sigma$). The chance probability, taking into account an appropriate trial factor, was estimated as 0.3%. Seven out of the 11 $\gamma$-ray events are clustered within 22 s, suggesting that the GRB timescale is $\sim 10$ s.

More recently, the Cherenkov telescope Milagrito (McEnery et al. 1999) detected an excess of events within the BATSE error box of GRB 970417a, with chance probability $2.8 \times 10^{-5}$. Since all the 54 GRBs detected by BATSE and falling in the Milagrito field of view have been examined, the chance probability of observing an excess with this significance in any of these bursts is $1.5 \times 10^{-3}$. Moreover, we note that the energy fluence of GRB 970417a may be explained with a source redshift $z \sim 0.7$ and an isotropic total energy in the TeV range, $\mathcal{E}^{iso}_{TeV} \gtrsim 10^{54}$ erg (Totani 2000).

From the above mentioned observations we can conclude that GRBs emit also in the GeV-TeV energy range, although only a fraction of the GRBs detected by BATSE have been observed at high-energy. This is consistent with the fact that high-energy $\gamma$-rays suffer serious attenuation due to the IIRF radiation, as discussed in Sect. 4.

In the framework of our model discussed in the previous sections, the possibility to detect high-energy GRB emission depends on the assumed model parameter values, in particular, on the GRB energetics $\mathcal{E}_p$, the cloud density $n_N$ and the magnetic field $B$.

A systematic study of the parameter range allowing detection through several experiments (in operation or planned) will be presented elsewhere. However, it is likely that the most suitable instrument to detect GRBs at energies $< 100$ GeV is the GLAST satellite, planned to be launched by NASA in 2005 (Gehrels & Michelson 1999).

Here, for illustrative purposes, we refer to the ARGO-YBJ (Astrophysical Radiation with Ground-based Observatory at YangBaJing) detector, under construction at the YangBaJing High Altitude Cosmic Ray Laboratory (Tibet, China). It is a cosmic-ray telescope optimized for the detection of small size

air shower and will be devoted to set several issues in cosmic-ray and astroparticle physics including, in particular, GRB physics in the energy range between $\simeq 50$ GeV and $\simeq$10 TeV (see Bacci et al. 1999 and Vernetto 1999).

GRBs are detectable at high-energy if the number $N_\gamma$ of air showers due to $\gamma$-rays from one burst is significant larger than the fluctuation $\sigma = \sqrt{N_b}$ of the background shower number $N_b$ due to cosmic-rays with arrival direction compatible with the burst position. So, in order to reduce the background and increase the detection sensitivity, a good angular resolution is of major importance (see Eqs. (17) and (18)).

The angular resolution of the ARGO apparatus $\psi_{70} \simeq 5^0$ (corresponding to $\epsilon = 0.7$) and the effective areas $A^{\gamma}_{eff}(E_\gamma)$ and $A^{CR}_{eff}(E_p)$, for $\gamma$-rays and cosmic-rays, respectively, have been numerically estimated through Montecarlo simulations by the ARGO collaboration (Surdo 2000)[6].

The number of events detectable by ARGO in the energy range $E_{min} - E_{max}$, during an observational time $T_{obs}$, is calculated by the following relations:

$$N_\gamma = \epsilon \int_{E_{min}}^{E_{max}} F_\gamma(E_\gamma; 0, T_{obs}) A^{\gamma}_{eff}(E_\gamma) dE_\gamma \qquad (17)$$

for the GRB signal and

$$N_b = 2\pi(1 - \cos\psi_{70}) T_{obs} \times \int_{E_{min}}^{E_{max}} \Phi^{CR}(E_p) A^{CR}_{eff}(E_p) dE_p \qquad (18)$$

for the cosmic-ray background. Here, the cosmic-ray flux $\Phi^{CR}(E_p)$ (in units of $\mathrm{cm}^{-2}\,\mathrm{s}^{-1}\,\mathrm{GeV}^{-1}\,\mathrm{sr}^{-1}$) is given by (Honda et al. 1995)

$$\Phi^{CR}(E_p) = \begin{cases} C_1\,(E_p + m_p)^{-2.585}\, e^{-\chi} & \text{for } E_p < 75\mathrm{GeV} \\ C_2\, E_p^{-2.75} & \text{for } E_p > 75\mathrm{GeV}\,, \end{cases} \qquad (19)$$

where $\chi = -1.871/(0.97 + \sqrt{E_p^2 - m_p^2})$, $C_1 = 1.085$ and $C_2 = 2.103$.

We take an energy range between $E_{min} = 10$ GeV and $E_{max} = 5$ TeV, although we have verified that our results do not change substantially if 1 GeV $\lesssim E_{min} \lesssim$ 50 GeV (due to the effective area suppression) and $E_{max} \gtrsim 5$ TeV (due to the signal and background flux suppression). In Fig. 7, assuming a detectability threshold condition of 4 standard deviations (i.e. $N_\gamma \geq 4\sqrt{N_b}$), we give $\mathcal{E}_p^{iso}$ as a function of $n_N$, for different intervals of observational time and for GRB redshift $z = 0.1$ (continuous lines), $z = 0.5$ (dashed lines) and $z = 1$ (dotted lines). Each curve defines the model parameter region above which a GRB should be detectable by ARGO apparatus, once the observational time and redshift are given. The horizontal line in Fig. 7 marks a conservative (low) value for $\mathcal{E}_p^{iso} = 10^{54}$ erg (corresponding to $\mathcal{E}_p \simeq 10^{53}\Delta\Omega$ erg). Nevertheless, a GRB at $z = 0.1$ produces a detectable high-energy $\gamma$-ray signal for any cloud density value $10^8\ \mathrm{cm}^{-3} \leq n_N \leq 10^{11}\ \mathrm{cm}^{-3}$, while if it lies at $z = 0.5$ a density $n_N \gtrsim 5 \times 10^9\ \mathrm{cm}^{-3}$ is needed. Even a GRB at $z = 1$ could be detectable provided $n_N \gtrsim 10^{11}\ \mathrm{cm}^{-3}$ and/or $\mathcal{E}_p^{iso} \gtrsim 10^{55}$ erg.

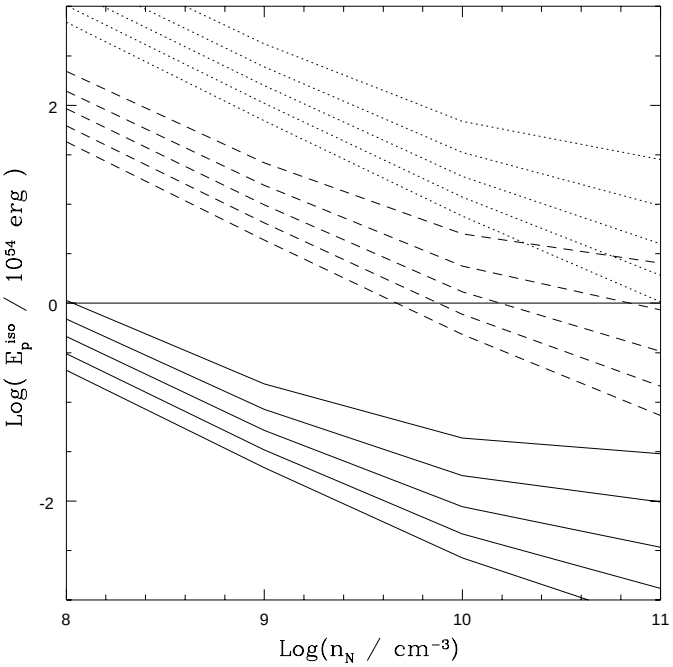


**Fig. 7.** The isotropic GRB energetics $\mathcal{E}_p^{iso}$ (in units of $10^{54}$ erg) is given as a function of $n_N$, for different intervals of observational time ($T_{obs} = 1,\ 10,\ 10^2,\ 10^3,\ 10^4$ s, from the bottom to the top) and GRB redshift $z = 0.1$ (continuous lines), $z = 0.5$ (dashed lines) and $z = 1$ (dotted lines). Each curve defines the model parameter region above which GRBs should be detectable by ARGO apparatus, once the observational time and source redshift are given.

## 6. Conclusions

In this paper we adopted Totani's proposal that GRB sources release roughly the same amount of energy $\mathcal{E} \simeq 10^{54}\Delta\Omega$ erg and that a substantial fraction of this energy is emitted in the form of accelerated protons coming out from the GRB source.

If there exists a dense enough cloud near or around the GRB source, protons, interacting with the nucleons in the cloud, give rise to pions and ultimately to a high-energy $\gamma$-ray signal (in the GeV-TeV energy band) within the error box of a GRB detected in the KeV - MeV energy band.

Due to the presence of magnetic fields (with assumed intensity $B \simeq 1\ \mu$G) around the source, i.e. within the proton propagation region before $pN$ interactions are in operation, the high-energy $\gamma$-ray signal results to be delayed and spread out over a longer time with respect to the soft $\gamma$-ray signal.

As it is shown in Fig. 3, the time duration of the $\gamma$-ray signal in the GeV - TeV energy band crucially depends on the cloud density $n_N$ and lasts much longer with respect to the signal in the soft $\gamma$-ray regime.

[6] In the energy range 100 GeV - 5 TeV the effective areas increase from $2 \times 10^7$ cm$^2$ to $9 \times 10^8$ cm$^2$, for $\gamma$-rays, and from $5 \times 10^6$ cm$^2$ to $8 \times 10^8$ cm$^2$, for CRs.

By assuming that the accelerated proton injection time $\Delta t$ is much shorter than the proton interaction time, we have calculated the $\gamma$-ray flux on Earth at different times starting from the onset of the high-energy signal and the corresponding fluences for different integration times. These quantities depend on both the cloud density $n_N$ and redshift $z$ of the GRB source. In particular, due to the $\gamma$-ray absorption from IIFR background radiation from stars and dust, the flux (and fluence) of the high-energy signal is largely suppressed for source distances $z > 1$.

In Sect. 5 we have analyzed the possibility to detect a GRB in the high-energy band referring, in particular, to the performances of the ARGO detector under construction in Tibet. As it can be seen from Fig. 7, there exists a wide range of values for the relevant model parameters $\mathcal{E}_p$ and $n_N$ which might make a GRB detectable in the high-energy band.

As far as the GRB occurrence rate is concerned, we rely on the analysis of the GRB space density done by Schmidt 1999 who assumed a homogeneous sample of GRB derived from BATSE DISCLA data and a wide variety of broken power-law GRB luminosity functions. As a result of this analysis, one obtains that about 13 GRB/yr are expected to occur at redshift $z \leq 0.5$ and $\sim 120$ GRB/yr at $z \leq 1$.

However, we note that a GRB with $z \sim 0.1$ is an extremely rare event (less than one GRB/yr). Moreover, it is expected that only a fraction of the GRB events meets the conditions to be observable on Earth since we do not claim that all bursts have $\mathcal{E}_p = 10^{54}\Delta\Omega$ erg and that accelerated protons interact with a very dense medium (with $10^8\mathrm{cm}^{-3} \leq n_N \leq 10^{11}\mathrm{cm}^{-3}$).

Finally, we note that, although the details of the target cloud geometry are not important as far as the high-energy $\gamma$-rays flux estimates, the long-wavelength afterglow crucially depends on that geometry. In particular, it is expected that a long-wavelength afterglow may accompany the high-energy $\gamma$-ray production only if the cloud covering factor is low enough.

*Acknowledgements.* We would like to thank the ARGO Group and in particular B. D'Ettorre, G. Mancarella, G. Marsella, A. Surdo and S. Vernetto for useful discussions.

## References

Abbrescia M., Bacci C., Barone F., et al., 1996, Proposal to the ARGO experiment, http://www1.na.infn.it/wsubnucl/cosm/argo/argo.html
Amenomori M., Cao Z., Dai B.Z., et al., 1996, A&A 311, 919
Bacci C., Barone F., Bartoli B., et al., 1998, Addendum to the ARGO Proposal, http://www1.na.infn.it/wsubnucl/cosm/argo/argo.html
Bacci C., Bao K. Z., Barone F., et al., 1999, A&AS 138, 597
Bednarz J., Ostrowski M., 1998, Phys. Rev. Lett. 80, 3911
Berezinskii V. S., Bulanov S. V., Dogiel V. A., et al., 1990, Astrophysics of Cosmic Rays Amsterdam: North-Holland
Böttcher M., Dermer C.D., 1998, ApJ 499, L131
Connaughton V., Akerlof C. W., Barthelmy S., et al., 1997, ApJ 479, 859
Costa E., Frontera F., Heise J., et al., 1997, Nat 387, 783
Dermer C.D., 1986, A&A 157, 223
Djorgovski S.G., Kulkarni, S.R., Bloom J.S., et al., 1998, ApJ 508, L17
Djorgovski S.G., Kulkarni, S.R., Bloom J.S., et al., 1999a, GCN Circ. 289, http://gcn.gsfc.nasa.gov/gcn/gcn3/289.gcn3
Djorgovski S.G., Kulkarni S.R., Bloom J.S., et al., 1999b, GCN Circ. 189
Eichler D., Livio M., Piran T., et al., 1989, Nat 340, 126
Freedman D.L., Waxman E., 1999, astro-ph 9912214
Fruchter A., 1999, ApJ 512, L1
Gaisser T.K., 1990, Cosmic Rays and Particle Physics Cambridge: Cambridge University Press
Galama T.J., Groot P.J., Vanparadijs J., et al., 1997, Nat 387, 479
Gehrels N., Michelson P., 1999, Astrop. Phys. 11, 277
Harrison F.A., Bloom J.S., Frail D.A., et al., 1999, ApJ 523, L121
Honda M., Kajita T., Kasahara K., et al., 1995, Phys. Rev. D 52, 4985
Huang Y. F., Dai Z. G., Lu T., 1999, astro-ph 0002433
Hurley K., Dingus B.L., Mukherjee R., et al., 1994, Nat 372, 652
Katz J.I., 1994, ApJ 432, L27
Kulkarni S.R., Djorgovski S.G., Ramaprakash A.N., et al., 1998, Nat 393, 35
Kulkarni S.R., Djorgovski S.G., Odewahn S.C., et al., 1999, Nat 398, 389
Kulkarni S.R., Berger E., Bloom J.S., et al., 2000, astro-ph 0002168
Lazzati D., Campana S., Ghisellini G., 1999, MNRAS 304, L31
McEnery J.E., Atkins R., Benbow W., et al., 1999, astro-ph 9910549
Meegan C.A., Pendleton G.N., Briggs M.S., et al., 1996, ApJS 106, 65
Metzger M.R., Djorgovski S.G., Kulkarni S.R., et al., 1997, Nat 387, 879
Mori M., 1997, ApJ 478, 225
Paciesas W.S., Meegan C.A., Pendleton G.N., et al., 1999, ApJS 122,465
Paczynski B., 1986, ApJ 308, L43
Paczynski B., 1998, ApJ 494, L45
Padilla L., Funk B., Krawczynski H., et al., 1998, A&A 337, 43
Particle Data Group, 1996, Phys. Rev. D 54
Pilla R.P., Loeb A., 1998, ApJ 494, L167
Piran T., 1999, Phys. Rep. 314, 575
Piro L., Costa E., Feroci M., et al., 1999, ApJ 514, L73
Rees M.J., Mészáros P., 1992, MNRAS 304, L31
Sagar R., Mohan V., Pandey A.K., et al., 2000, astro-ph 0003257
Salomon M.H., Stecker F.W., 1998, ApJ 493, 547
Sazonov S.Y., Sunyaev R.A., Terekhov O.V., et al., 1998, A&AS 129, 1
Schneid E.J., Bertsch D.L., Fichtel C.E., et al., 1992, A&A 255, L13
Schneid E.J., Bertsch D.L., Dingus B.L., et al., 1995, ApJ 453, 95
Schmidt M., 1999, ApJ 523, L117
Stecker F.W., De Jager O.C., 1997, ApJ 476, 712
Stephens A., Badhwar G.D., 1981, Ap&SS 76, 213
Surdo A., 2000, private communication
Totani T., 1998a, ApJ 502, L13
Totani T., 1998b, ApJ 509, L81
Totani T., 1999, MNRAS 307, L41
Totani T., 2000, astro-ph 0005071
ARGO-YBJ Collaboration (presented by Vernetto S.), 1999, astro-ph 9906185
Vernetto S., 2000, Astrop. Phys. 13, 75
Vietri M., 1995, ApJ 453, 883
Vietri M., 1997, Phys. Rev. Lett. 78, 4328
Vietri M., Stella L., 1998, ApJ 507, L45
Vietri M., 2000, astro-ph/0002269
Waxman E., 1995, Phys. Rev. Lett. 75, 386
Woosley S.E., 1993, ApJ 330,218
Yoshida A., Namiki M., Otani C., et al., 1999, A&AS 138, 433